






The electronic structure of β -Ga₂O₃

Cite as: APL Mater. 7, 022522 (2019); <https://doi.org/10.1063/1.5054395>

Submitted: 31 August 2018 . Accepted: 17 December 2018 . Published Online: 22 January 2019

M. Mulazzi , F. Reichmann, A. Becker, W. M. Klesse, P. Alippi , V. Fiorentini , A. Parisini, M. Bosi , and R. Fornari 



View Online



Export Citation



CrossMark



Measure Ready
M91 FastHall™ Controller

A revolutionary new instrument
for complete Hall analysis



The electronic structure of ε -Ga₂O₃

Cite as: APL Mater. 7, 022522 (2019); doi: 10.1063/1.5054395

Submitted: 31 August 2018 • Accepted: 17 December 2018 •

Published Online: 22 January 2019



M. Mulazzi,^{1,2}  F. Reichmann,³ A. Becker,³ W. M. Klesse,³ P. Alippi,⁴  V. Fiorentini,^{5,6}  A. Parisini,⁷
M. Bosi,⁸  and R. Fornari^{7,8} 

AFFILIATIONS

¹Institut für Physik, Humboldt-Universität zu Berlin, Newtonstr. 15, D-12489 Berlin, Germany

²Leibniz-Institut für Kristallzüchtung, Max-Born-Str. 2, D-12489 Berlin, Germany

³IHP, Im Technologiepark 25, D-15236 Frankfurt (Oder), Germany

⁴CNR-ISM, Via Salaria km 29,300, I-00015 Monterotondo Stazione (Rome), Italy

⁵Department of Physics, Cagliari University, I-09042 Monserrato (CA), Italy

⁶CNR-IOM, UOS Cagliari University, I-09042 Monserrato (CA), Italy

⁷Department of Mathematical, Physical and Computer Sciences, Parma University, Viale delle Scienze 7/A, I-43124 Parma, Italy

⁸CNR, Institute of Electronic and Magnetic Materials, Viale delle Scienze 37/A, I-43124 Parma, Italy

ABSTRACT

The electronic structure of ε -Ga₂O₃ thin films has been investigated by *ab initio* calculations and photoemission spectroscopy with UV, soft, and hard X-rays to probe the surface and bulk properties. The latter measurements reveal a peculiar satellite structure in the Ga 2p core level spectrum, absent at the surface, and a core-level broadening that can be attributed to photoelectron recoil. The photoemission experiments indicate that the energy separation between the valence band and the Fermi level is about 4.4 eV, a valence band maximum at the Γ point and an effective mass of the highest lying bands of ~ 4.2 free electron masses. The value of the bandgap compares well with that obtained by optical experiments and with that obtained by calculations performed using a hybrid density-functional, which also reproduce well the dispersion and density of states.

© 2019 Author(s). All article content, except where otherwise noted, is licensed under a Creative Commons Attribution (CC BY) license (<http://creativecommons.org/licenses/by/4.0/>). <https://doi.org/10.1063/1.5054395>

Gallium oxide (Ga₂O₃) is a wide bandgap transparent semiconducting oxide (TCO). Although known for decades, it is only in the last ten years that it received a lot of attention as a novel wide bandgap semiconductor for power electronic and deep-UV applications. Among five crystal structures of Ga₂O₃, the monoclinic β phase is the most thermodynamically stable and indeed the only one that can be grown from a Ga₂O₃ melt, either by Czochralski¹ or Edge-defined Film-fed Growth (EFG).² Specific advantages of this material are the bandgap close to 5 eV, transparency up to the UV-C range, and very high breakdown voltage. Relatively high n-type conductivity can be achieved by doping with Si, Sn, or Ge, which makes β -Ga₂O₃ suitable for fabrication of power transistors,³ high-voltage diodes,⁴ and UV photodetectors.⁵

The ε phase of Ga₂O₃, object of the present investigation, is the second most stable, after β , and was observed to be thermodynamically (meta)stable up to about 700 °C exhibiting

a complete transition to β around 900 °C.⁶ This polymorph can easily be deposited on commercial c-oriented sapphire at temperatures much lower than those needed for β -Ga₂O₃.⁷ In addition to having an orthorhombic (pseudo-hexagonal) crystallographic structure⁸ and a wide bandgap of about 4.6 eV,⁹ ε -Ga₂O₃ presents unique properties such as ferroelectric behavior¹⁰ with a relatively large spontaneous polarisation,¹¹ making this polymorph even more interesting, as it might be exploited to obtain a two-dimensional electron gas and thus high mobility devices.

Many angle-resolved photoemission spectroscopy (ARPES) studies have already been devoted to TCOs, ZnO,¹²⁻¹⁵ CdO,¹⁶⁻¹⁸ and In₂O₃,¹⁹⁻²¹ and also to β -Ga₂O₃.²²⁻²⁵ However, such an investigation is still lacking for ε -Ga₂O₃. The interesting properties of the ε phase, on the other hand, fully justify the investigation of its electronic structure and motivate our present ARPES investigation. In the following, we report on the

band structure of ϵ -Ga₂O₃ grown in the form of thin films of 250 nm thickness. ARPES excited with low- and high-energy photons was used to measure the core-levels as well as the valence band with high momentum resolution. The films are electrically conductive and stable against the sputtering and annealing procedure that we applied to clean the surface.

The ϵ -Ga₂O₃ thin films were grown by Metal-Organic Chemical Vapor Deposition (MOCVD) on 2-inches (0001) oriented sapphire by using the growth parameters reported in the literature.⁷ The films were doped with diluted silane to get high conductivity (the resistivity of samples from the same wafer was 0.8-1 Ω cm and carrier concentration was $2\text{--}3 \times 10^{18}$ cm⁻³), which prevented the charging effects that were previously observed in undoped ϵ -Ga₂O₃ epilayers.

The measurements were carried out at the surface cluster of the Institute for High-Performance Microelectronics (IHP), featuring a SPECS Phoibos 150 electron spectrometer. The photons used for the ARPES experiment are generated by a monochromatised He discharge lamp, while a monochromatised X-ray tube with aluminum and silver targets was used to obtain the Al K α and Ag L α emission lines at photon energies of $h\nu_{\text{Al}} = 1468.7$ eV and $h\nu_{\text{Ag}} = 2984.3$ eV, respectively. Prior to photoelectron spectroscopy, the surface of the films was prepared by repeated Ar ion sputtering and annealing cycles. While at the beginning an ion energy of 1 keV was used, at later stages, it was reduced to 500 eV to avoid excessive material removal. For the same reason, namely, the limited film thickness, the samples were sputtered 5 min per cycle. The films were heated at 500 °C for 30 min, a temperature at which no transition between the ϵ and β phases occurs. All measurements were taken at room temperature, and the pressure in the chamber during the measurements was lower than 2×10^{-10} mbar and about 5×10^{-9} mbar during the annealing.

X-ray photoemission spectroscopy (XPS) is a refined and relatively easy technique that can be used to investigate the electronic structure of materials. While its main purpose is the identification of the chemical species in a compound, it has recently been applied to quantitatively determine the band bending in a semiconductor.²⁶ In comparison with this work in which UV radiation was used, X-rays were employed in the present study since they possess two advantages: measurements (1) of several core levels from either gallium or oxygen

and (2) of many values of the mean escape depth are possible. The bulk sensitivity is enhanced even more by the use of the higher photon energy $h\nu_{\text{Ag}}$ imparting higher kinetic energy to the photoelectrons.

Figure 1 shows the spectrum of ϵ -Ga₂O₃ taken with the Al K α radiation, $h\nu_{\text{Al}}$.

All measured photoemission and Auger peaks of the spectrum of Fig. 1 could unambiguously be identified. These are the very first photoemission measurements on the ϵ phase thin films. We stress that we observed no peaks from either aluminum or silicon, which has three implications: (i) the Ar sputtering cycles just removed a thin Ga₂O₃ surface layer so that no substrate portions resulted exposed to X-rays and (ii) no Al migration from the substrate to epilayer occurred during the annealing. Moreover, (iii) the small amount of Si introduced via silane doping during growth must be well below the XPS detection limit ($\approx 0.1\%$). In fact, the absence of any Si core-level peaks indicates that there is no Si surface segregation in the layers.

Next, we wish to discuss the Ga 2p core levels (the strongest lines measured) and the O 1s. With the intention of detecting differences between the surface and the bulk, we used the two photon energies mentioned above. Furthermore, for the Al K α case, we repeated measurements at two emission angles, namely, normal emission (labeled as 0°) and at 70° from normal emission, i.e., at a grazing emission angle of 20°.

The reason for the use of a grazing angle is to increase the surface sensitivity by effectively projecting the inelastic mean free path (IMFP) on the surface normal direction, reducing it by a factor $\cos(\theta)$. For $\theta = 70^\circ$, this equals $\cos(70^\circ) \approx 0.342$.

The first interesting feature observed in Fig. 2(a) is the appearance of two weak satellites when the photon energy is increased. Contrary to the spectra taken with $h\nu_{\text{Al}}$, the spectrum taken with $h\nu_{\text{Ag}}$ shows a distinct peak at a binding energy of -1110 eV, lower than that of the Ga 2p_{3/2} peak. Furthermore, at -1130 eV binding energy, there is a second peak, also absent in the spectra taken with $h\nu_{\text{Al}}$. The importance of these two peaks lies in their energy difference relative to the Ga 2p_{3/2} and Ga 2p_{1/2} peaks. In fact, the Ga 2p is split in the final state by spin-orbit coupling by about 26.8 eV, and thus, every peak observed at an energy ΔE from 3/2 peak should be replicated and located at a ΔE energy from the 1/2 peak.

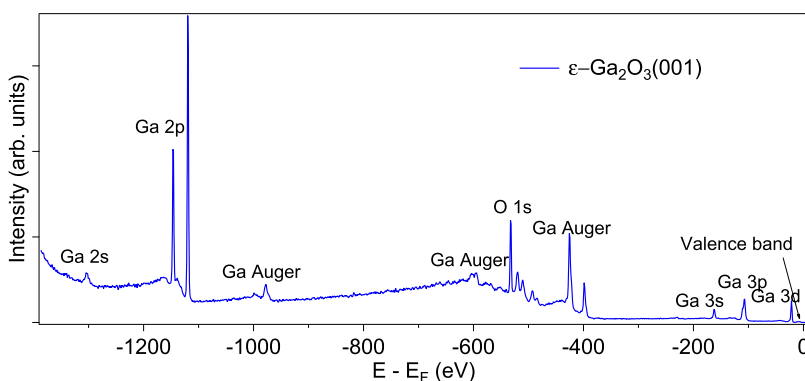


FIG. 1. XPS spectrum in a wide binding energy range measured at a photon energy $h\nu_{\text{Ag}}$. All core levels have been identified, as well as a number of Auger peaks located at about -950 eV and in the -800 eV to -400 eV range. In this range, the Auger peaks overlap with the O 1s core level at -534 eV. The black arrow indicates a very weak peak near zero binding energy, which is the valence band. The latter is hardly visible in XPS but is thoroughly investigated with the He I radiation.

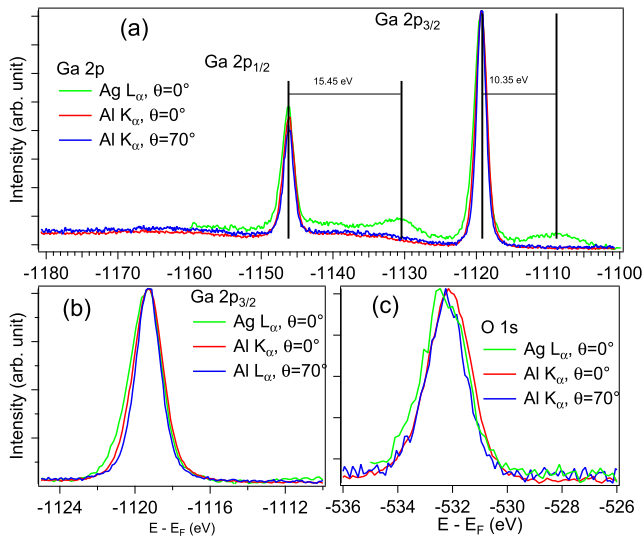


FIG. 2. Core-level measurements taken at different photon energies and emission angles, as indicated in the figure labels. (a) shows the spectrum of the 2p core level doublet split by spin-orbit coupling; (b) the $2p_{3/2}$ component and (c) the O 1s core level.

Thus, the peak at -1110 eV, located 10.35 eV above the Ga $2p_{3/2}$, should be replicated 10.35 eV above the $1/2$ component. However, the peak positioned between the Ga $2p_{3/2}$ and Ga $2p_{1/2}$ lines is at 15.45 eV from the Ga $2p_{1/2}$ component and therefore is not a replica but a further satellite.

While most of the photoemission satellites lie at the left of the main line, i.e., at lower kinetic energies and apparently higher binding energies, the peak at -1130 eV lies on the right side, i.e., at higher kinetic energies. The attribution of this peak is not unambiguous as two possibilities are available, i.e., a non-local screening as it happens in manganites or a shake-down satellite, occurring when the photohole pulls electrons below the Fermi level in the final-state, leading to a more effective valence electron screening of the hole. However, in all previously studied systems,^{27–30} the well-screened peaks appear only a few eV from the main line, but in our case, the difference is more than 10 eV, which is of the scale of the typical correlation energy in oxides. Therefore, we tend to believe that the satellite derives from a shake-down effect.

Figures 2(b) and 2(c) show zoomed-in images of the Ga $2p_{3/2}$ and O 1s peaks in a narrow energy range. The qualitative behavior of the peaks upon photon energy and emission angle is the same. In fact, the binding energy of the peaks taken with $h\nu_{Al}$ does not change upon a variation of the emission angle. However, the width of the peaks taken in the most surface sensitive conditions (the blue lines in Fig. 2) is slightly narrower than those measured at normal emission, which is more bulk sensitive. The measurements taken with $h\nu_{Ag}$, which are even more bulk sensitive, are broader and show an asymmetric tail on the left side. We attribute the left tail of the peaks taken at high energy at normal emission ($\theta = 0^\circ$) to the recoil effect occurring in core-level peaks taken at high photon energy:^{30,31} a hard X-ray can excite a photoelectron to

such high kinetic energies that, by momentum conservation, the ion left behind by the photoelectron is set in motion. The shift and asymmetric broadening of the photoemission peaks appears because the ion dissipates its energy to the lattice by phonon emission.

The electronic bands of ϵ -Ga₂O₃ have been calculated, after structural optimisation, within density-functional theory both in the generalized gradient approximation³² (GGA) and the hybrid-functional³³ (HSE) approach, using the projector augmented wave method as implemented in the VASP code.³⁴ For Ga, we used the 13-electron “Ga-d” VASP PAW dataset with $3d$ states in the valence and two projectors in the s , p , and d channels and one f projector; for O, we used the 6-electron “O” VASP PAW dataset with two projectors in the s and p channels and one in the d channel. The energy cutoff is 400 eV, and the k -point mesh is $4 \times 2 \times 2$ for self-consistency and optimization and $8 \times 6 \times 6$ for the calculation of the density of states (DOS). The parameters $\alpha = 0.25$ and $\mu = 0.2$ are used in HSE.

ϵ -Ga₂O₃ has a non-magnetic 40-atom unit cell. The valence manifold thus comprises 72 spin-degenerate bands that fall nicely in the experimental energy range. The total valence band width is 6.96 eV and 7.26 eV in GGA and HSE, respectively. The occupied bands are rather flat, while the first conduction band (CB) disperses strongly. The conduction band minimum (CBM) is at Γ , and the gap is, as expected, underestimated by GGA (2.32 eV), whereas HSE yields 4.26 eV, comparable to the experiment. Previous calculations³⁵ using the B3LYP functional reported 4.62 eV, but any comparison of different beyond-local-DFT approaches carries uncertainties of order ± 0.5 eV, as shown, e.g., for β -Ga₂O₃.³⁶ The present ARPES experiments suggest (see below) a lower bound of 4.41 eV; photoconductivity and optical absorption indicate a value of about 4.6 eV.⁹

The experimental valence band dispersion is presented in Fig. 3(a) in a false-colour scale, as explained in the caption.

The data show that the valence band consists of a single rather broad band located 6 eV below the Fermi level (the zero of the y -scale in the left panel of Fig. 3) which reaches its minimum binding energy at the Γ point of the Brillouin zone. The binding energy of the band increases with the wave-vector, indicating a negative high effective mass. To obtain the latter, we extracted EDCs at 0.05 \AA^{-1} steps across the whole wave-vector range and fitted the spectra from -7 eV to -3 eV to obtain the binding energy of the maximum. Then we fitted the data with a parabola and obtained an effective mass $m^* = -4.2$ electron masses. Thus, the effective mass is negative and large, and the bands are fairly flat. The resulting parabola is indicated by the red line superimposed to the band-structure calculations in the right panel of Fig. 3. As shown in Fig. 3, a large number of theoretical bands lie in the same energy range of the experimental signal, with a few dispersive bands overlapping with many flat ones, especially near the valence band maximum (VBM). The result of the calculations shown in Fig. 3 confirms that the GGA bandgap underestimates the experimental one, as mentioned.

The question of the characteristics of the bandgap cannot be addressed by ARPES, unless the CB is partially filled. Only

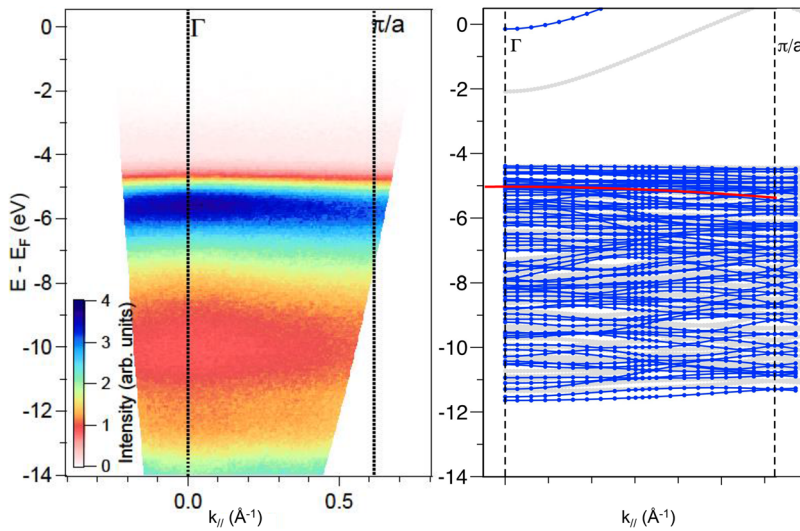


FIG. 3. (Left) ARPES map in false colours (as indicated by the linear colour scale) taken with the photon energy $h\nu = 21.2$ eV. The strong intensity at about -6 eV is due to the oxygen states dispersing to higher binding energies with momentum. (Right) Theoretical electronic bands within the GGA (gray continuous lines) and HSE (blue dotted lines) approximations, with the valence band top of both aligned with the experimental one at Γ . A parabolic band (red continuous line) is superimposed, with a mass of $-4.2 m_0$ [as determined by fitting the experimental Energy Distribution Curves (EDCs)].

in this case, the position of the CBM in k -space can be directly observed. The experimental data show no intensity near the Fermi level [the zero for the energy scale in Fig. 3(a)], leading us to the conclusion that the CBM is not occupied. According to our calculations, as well as previous ones,³⁵ the CBM is at the Γ point. The experimental data suggest that the VBM is at or near (see Fig. 5) the zone centre, so ϵ -Ga₂O₃ is likely a direct-gap semiconductor.

Figure 4(a) shows the EDC taken at zero k_{\parallel} [vertical dashed line in Fig. 3(a)], which has been used to extract the size of the single-particle bandgap. The peak region and the right flank of the EDC have been fitted to obtain the inflexion point, from which a linear extrapolation to zero has been used to estimate the apparent bandgap, obtaining $E_B = 4.41$ eV. This compares well with optical measurements on undoped as-grown films,⁹ suggesting that (a) the Fermi level is pinned some 0.2 eV below the CBM and (b) correlation effects in optical experiments are small.

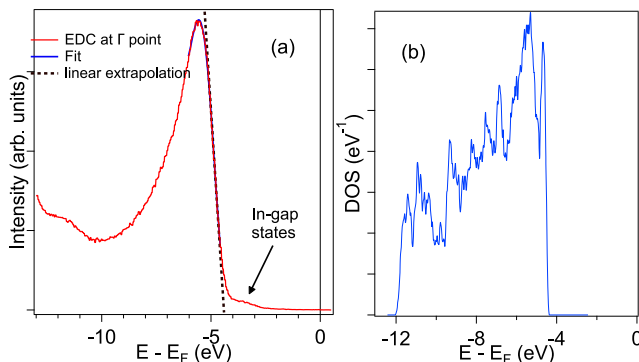


FIG. 4. (a) Experimental EDC taken at the Γ point superimposed to a fit of the spectrum used to do the linear extrapolation. (b) The theoretical calculation of the density of states, smoothed to better indicate the most prominent features, obtained with the hybrid functional.

Surprisingly, a weak shoulder peak is observed [Fig. 4(a)] inside the bandgap at about 3.5 eV below E_F . Its origin is unknown, but we associate it with localised native-defect states because of its almost vanishing dispersion and of similar observations made in other oxide systems.^{37–39} The theoretical density of states in Fig. 4 finds no state in that region, supporting an extrinsic origin of this peak.

A direct comparison between theory and experiment is presented in Fig. 4, where the theoretical DOS and the experimental EDC at the Γ point are shown. Although the DOS is k -integrated, while the EDC is measured at a single k , the validity of the comparison is supported by the flatness of the bands. Indeed, the comparison relates fairly satisfactorily the computed occupations and observed intensities: in both cases, a dominant asymmetric peak is observed, topping at about -6 eV and spanning a roughly 5 eV-wide interval, with a major dip around -10 eV; the intensity then picks up again, peaking at -11 eV. The theoretical DOS ends at -11.5 eV, while the experimental one has a plateau at that energy, before increasing again toward higher binding energies. This latter intensity increase is due to the secondary electron background and not to primary photoelectrons. However, the peak at -11 eV is a genuine feature, unrelated to the Ga 3d core levels. The binding energy of the Ga 3d is 21 eV from the Fermi level, in good agreement with the predictions of both GGA and HSE, i.e., -20.2 eV and -21.9 eV below the same reference.

Concerning transport band masses and the characteristics of the gap, two points stand out upon a closer look (Fig. 5) at the highest valence bands. First, the gap is direct according to the more accurate HSE approach, which predicts a VBM at the Γ point (in accordance with the experiment). GGA would instead predict that the very flat top band has a local minimum at Γ and a maximum at $k_{\parallel} = 0.35 \text{ \AA}^{-1}$, hence a (barely) indirect band structure.

Second, although the main peak in the EDC centered around -5 eV provides, as mentioned earlier, an average

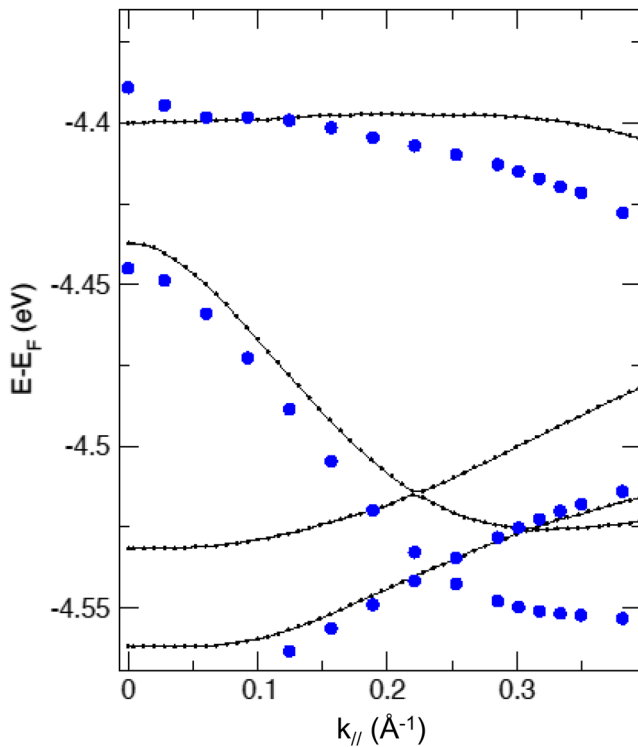


FIG. 5. Calculation of the bands near the VBM plotted from Γ along the experimentally explored direction with the GGA (black lines) and the HSE (blue dots).

valence mass of $-4.2 m_e$, the mass adopted by p carriers doped into the material will be that of the highest band (which, it is simple to estimate, is the only one that will be occupied for any reasonable carrier concentration, say below 10^{21} cm^{-3}). Fitting a parabola to the highest computed HSE band in the experimentally explored direction, we find a very large effective mass of $-15 m_e$. Another likely occurrence we have not explored explicitly here is that the top valence band will probably be significantly anisotropic and will need to be described by more complex datasets such as Luttinger parameters.

The electronic structure of $\varepsilon\text{-Ga}_2\text{O}_3$ films grown by MOCVD on c -oriented sapphire was investigated by XPS and ARPES. The main conclusions are that no band bending is observed, which excludes the presence of a large density of surface states. However, a careful check of the ARPES map shows an accumulation of states at about 3.5 eV from the Fermi level. These states are possibly related to intrinsic defects, but more comparative studies (for instance, on samples grown with different O-to-Ga ratios in the vapour phase) are necessary to clarify this question.

Our ARPES investigations indicate a weak maximum of the valence band at the Γ point, therefore strongly hinting that the ε -phase is indeed a direct bandgap semiconductor, although ARPES alone cannot supply a full confirmation since it cannot measure the CBM position. The effective mass for holes in the top of the VB was estimated to be about $-4.2 m_0$.

Theory reproduces rather well the experimental intensities and predicts the CBM as well as (in its arguably most accurate version) the VBM at Γ , with a gap not far from the experiment.

The authors wish to thank Professor A. Bosio, Dr. V. Montedoro, G. Garulli, A. Gorreri, and S. Vantaggio for their support in making ohmic contacts and electrical measurements of doped Ga_2O_3 epilayers and Professor Dr. C. Wenger for allowing the use of the surface science cluster.

This work was supported in part by UniCA, Fondazione di Sardegna, Regione Sardegna via Progetto biennale di ateneo 2016 *Multiphysics approach to thermoelectricity*, and CINECA-ISCRA grants.

REFERENCES

- Y. Tomm, P. Reiche, D. Klimm, and T. Fukuda, *J. Cryst. Growth* **220**, 510–514 (2000).
- A. Kuramata, K. Koshi, S. Watanabe, Y. Yu, T. Masui, and S. Yamakoshi, *Jpn. J. Appl. Phys., Part 1* **55**, 1202A2 (2016).
- M. Higashiwaki, K. Sasaki, H. Murakami, Y. Kumagai, A. Koukitu, A. Kuramata, T. Masui, and S. Yamakoshi, *Semicond. Sci. Technol.* **31**, 034001 (2016).
- M. A. Rozhkov, E. S. Kolodeznyi, A. M. Smirnov, V. E. Bougrov, and A. E. Romanov, *Mater. Phys. Mech.* **24**, 194–200 (2015).
- M. Zhong, Z. Wei, X. Meng, F. Wu, and J. Li, *J. Alloys Compd.* **619**, 572–575 (2015).
- R. Fornari, M. Pavesi, V. Montedoro, D. Klimm, F. Mezzadri, I. Cora, B. Péc, F. Boschi, A. Parisini, A. Baraldi, C. Ferrari, E. Gombia, and M. Bosi, *Acta Mater.* **140**, 411–416 (2017).
- F. Boschi, M. Bosi, T. Berzina, E. Buffagni, C. Ferrari, and R. Fornari, *J. Cryst. Growth* **443**, 25–30 (2016).
- I. Cora, F. Mezzadri, F. Boschi, M. Bosi, M. Caplovicova, G. Calestani, I. Dodony, B. Péc, and R. Fornari, *CrystEngComm* **19**, 1509 (2017).
- M. Pavesi, F. Fabbri, F. Boschi, G. Piacentini, A. Baraldi, M. Bosi, E. Gombia, A. Parisini, and R. Fornari, *Mater. Chem. Phys.* **205**, 502–507 (2018).
- F. Mezzadri, G. Calestani, F. Boschi, D. Delmonte, M. Bosi, and R. Fornari, *Inorg. Chem.* **55**, 12079–12084 (2016).
- M. B. Maccioni and V. Fiorentini, *Appl. Phys. Express* **9**, 041102 (2016).
- R. A. Powell, W. E. Spicer, and J. C. McMenamin, *Phys. Rev. B* **6**, 3056 (1972).
- K. Ozawa, Y. Oba, K. Edamoto, M. Higashiguchi, Y. Miura, K. Tanaka, K. Shimada, H. Namatame, and M. Taniguchi, *Phys. Rev. B* **79**, 075314 (2009).
- L. F. J. Piper, A. R. H. Preston, A. Fedorov, S. W. Cho, A. DeMasi, and K. E. Smith, *Phys. Rev. B* **81**, 233305 (2010).
- R. Yukawa, K. Ozawa, S. Yamamoto, H. Iwasawa, K. Shimada, E. F. Schwier, K. Yoshimatsu, H. Kumigashira, H. Namatame, M. Taniguchi, and I. Matsuda, *Phys. Rev. B* **94**, 165313 (2016).
- P. D. C. King, T. D. Veal, C. F. McConville, J. Zuniga-Pérez, V. Muñoz-Sanjosé, M. Hopkinson, E. D. L. Rienks, M. F. Jensen, and Ph. Hofmann, *Phys. Rev. Lett.* **104**, 256803 (2010).
- J. J. Mudd, T.-L. Lee, V. Muñoz-Sanjosé, J. Zuniga-Pérez, D. Hesp, J. M. Kakh, D. J. Payne, R. G. Egdell, and C. F. McConville, *Phys. Rev. B* **89**, 035203 (2014).
- J. J. Mudd, T.-L. Lee, V. Muñoz-Sanjosé, J. Zuniga-Pérez, D. J. Payne, R. G. Egdell, and C. F. McConville, *Phys. Rev. B* **89**, 165305 (2014).
- K. H. L. Zhang, R. G. Egdell, F. Offi, S. Iacobucci, L. Petaccia, S. Gorovikov, and P. D. C. King, *Phys. Rev. Lett.* **110**, 056803 (2013).
- C. Körber, V. Krishnakumar, A. Klein, G. Panaccione, P. Torelli, A. Walsh, J. L. F. Da Silva, S.-H. Wei, R. G. Egdell, and D. J. Payne, *Phys. Rev. B* **81**, 165207 (2010).

- ²¹V. Scherer, C. Janowitz, A. Krapf, H. Dwelk, D. Braun, and R. Manzke, *Appl. Phys. Lett.* **100**(21), 212108 (2012).
- ²²M. Mohamed, C. Janowitz, I. Unger, R. Manzke, Z. Galazka, R. Uecker, R. Fornari, J. R. Weber, J. B. Varley, and C. G. Van de Walle, *Appl. Phys. Lett.* **97**, 211903 (2010).
- ²³M. Mohamed, I. Unger, C. Janowitz, R. Manzke, Z. Galazka, R. Uecker, and R. Fornari, *J. Phys.: Conf. Ser.* **286**(1), 012027 (2011).
- ²⁴C. Janowitz, V. Scherer, M. Mohamed, A. Krapf, H. Dwelk, R. Manzke, Z. Galazka, R. Uecker, K. Irmscher, R. Fornari, M. Michling, D. Schmeier, J. R. Weber, J. B. Varley, and C. G. Van de Walle, *New J. Phys.* **13**, 085014 (2011).
- ²⁵M. Mohamed, K. Irmscher, C. Janowitz, Z. Galazka, R. Manzke, and R. Fornari, *Appl. Phys. Lett.* **101**(13), 132106 (2012).
- ²⁶B. Thielert, C. Janowitz, Z. Galazka, and M. Mulazzi, *Phys. Rev. B* **97**, 235309 (2018).
- ²⁷K. Horiba, M. Taguchi, A. Chainani, Y. Takata, E. Ikenaga, D. Miwa, Y. Nishino, K. Tamasaku, M. Awaji, A. Takeuchi, M. Yabashi, H. Namatame, M. Taniguchi, H. Kumigashira, M. Oshima, M. Lippmaa, M. Kawasaki, H. Koinuma, K. Kobayashi, T. Ishikawa, and S. Shin, *Phys. Rev. Lett.* **93**, 236401 (2004).
- ²⁸M. Sperlich, C. König, G. Güntherodt, A. Sekiyama, G. Funabashi, M. Tsunekawa, S. Imada, A. Shigemoto, K. Okada, A. Higashiya, M. Yabashi, K. Tamasaku, T. Ishikawa, V. Renken, T. Allmers, M. Donath, and S. Suga, *Phys. Rev. B* **87**, 235138 (2013).
- ²⁹M. Taguchi, A. Chainani, N. Kamakura, K. Horiba, Y. Takata, M. Yabashi, K. Tamasaku, Y. Nishino, D. Miwa, T. Ishikawa, S. Shin, E. Ikenaga, T. Yokoya, K. Kobayashi, T. Mochiku, K. Hirata, and K. Motoya, *Phys. Rev. B* **71**, 155102 (2005).
- ³⁰*Hard X-Ray Photoelectron Spectroscopy (HAXPES)*, edited by J. Woicik (Springer, Heidelberg, 2016).
- ³¹Y. Takata, Y. Kayanuma, M. Yabashi, K. Tamasaku, Y. Nishino, D. Miwa, Y. Harada, K. Horiba, S. Shin, S. Tanaka, E. Ikenaga, K. Kobayashi, Y. Senba, H. Ohashi, and T. Ishikawa, *Phys. Rev. B* **75**, 233404 (2007).
- ³²J. P. Perdew, M. Ernzerhof, and K. Burke, *J. Chem. Phys.* **105**, 9982 (1996).
- ³³J. Heyd, G. E. Scuseria, and M. Ernzerhof, *J. Chem. Phys.* **118**, 8207 (2003).
- ³⁴G. Kresse and J. Furthmüller, *Phys. Rev. B* **54**, 11169 (1996); G. Kresse and D. Joubert, *ibid.* **59**, 1758 (1999).
- ³⁵J. Kim, D. Tahara, Y. Miura, and B. G. Kim, *Appl. Phys. Express* **11**, 061101 (2018).
- ³⁶F. Ricci, F. Boschi, A. Baraldi, A. Filippetti, M. Higashiwaki, A. Kuramata, V. Fiorentini, and R. Fornari, *J. Phys.: Condens. Matter* **28**, 224005 (2016).
- ³⁷Y. Aiura, I. Hase, H. Bando, T. Yasue, T. Saitoh, and D. S. Dessau, *Surf. Sci.* **515**, 61 (2002).
- ³⁸A. F. Santander-Syro, C. Bareille, F. Fortuna, O. Copie, M. Gabay, F. Bertran, A. Taleb-Ibrahimi, P. Le Fèvre, G. Herranz, N. Reyren, M. Bibes, A. Barthlmy, P. Lecoeur, J. Guevara, and M. J. Rozenberg, *Phys. Rev. B* **86**, 121107(R) (2012).
- ³⁹S. Backes, T. C. Rödel, F. Fortuna, E. Frantzeskakis, P. Le Fèvre, F. Bertran, M. Kobayashi, R. Yukawa, T. Mitsuhashi, M. Kitamura, K. Horiba, H. Kumigashira, R. Saint-Martin, A. Fouchet, B. Berini, Y. Dumont, A. J. Kim, F. Lechermann, H. O. Jeschke, M. J. Rozenberg, R. Valentí, and A. F. Santander-Syro, *Phys. Rev. B* **94**, 241110(R) (2016).